Kondo-Majorana coupling in Double Quantum Dots.

by

Jesús David Cifuentes Pardo

Advisor: Luis Gregorio Dias da Silva

MASTER OF SCIENCE

in

Instituto de Física

(Condensed Matter Physics)

UNIVERSIDADE DE SÃO PAULO

(R. do Matão, 1371 - Butantã, São Paulo)

February 18, 2019

Chapter 1

Abstract

In the last decades the interest in the "search of Majorana fermions" in condensed matter systems [1] has increased due to their potential applications in quantum computing. As recently as 2012, experimental works reporting the detection of such quasiparticles [2, 3]. Later works [4, 5, 6, 7], including a recent paper published by the advisor of this dissertation and collaborators [8], set out to explore the interplay of such Majorana zero-modes with strongly interacting systems such as semiconductor quantum dots, which can be readily integrated in the device. This research project aims to expand this idea using the numerical renormalization group to study the model of a double quantum dot coupled to metallic leads and to a topological superconductor supporting edge Majorana zero modes (MZMs). This simple model allows the manipulation of the MZMs bringing possible applications to braiding procedures . In addition, we will study the interplay of Kondo correlations, exchange interactions and Majorana physics.

Chapter 2

Table of Contents

Chapter 3

The Pursuit of Majorana Fermions

> *"It started out with a toy model demonstration, and then I realized it was very good model. You don't understand the full implications until other people start thinking it is true and they observe the big picture [...] Now, that toy model is like Hydrogen atom for topological materials- it turned out to be the first example of topological quantum matter."*
>
> *– F. Duncan M. Haldane*

The Majorana Fermions, so called in the name of the Italian physicist Ettore Majorana, were first proposed as the real solution of the Dirac equation. The real field that solves this equation describes a fermion which is its own antiparticle, thus it has no electric charge nor mass. Till these days, no fundamental particle with these characteristics has been observed. However, the last decade has been full of excitement as new Majorana quasi-particles have been observed at the edges of topological superconductors.

The topological superconductors, belong to an emergent group of materials that experience phase transitions without passing through a symmetry breaking, hence they cannot be characterized by Landau theory. Instead, these phases of matter are described by a new type of order determined by the topology of the Brilloin zone. In mathematics, topology is used to describe non-local features of surfaces (or manifolds) that are preserved under smooth deformations. The cliché, but always educative, joke to explain this concept says that "Topologist cannot tell the difference between a donut and a coffee cup, since one of them can always be continuously deformed into the other through a sequence of smooth, small alterations" (Figure 3.1).[1] However

[1] For decades, this has been the mean reason for the absence of donuts at topology workshops.

Figure 3.1: Coffe-donut: adiabatic evolution

it wouldn't be possible to deform soccer ball into a donut since no there is no way of making 'softly' a hole into the ball.

The insight of topology into the field of condensed matter physics is that those materials that are attributed a topological characterization are endowed with a characteristic stability under smooth deformations (adiabatic evolutions) . The most famous example of this behavior is the integer quantum hall effect (IQHE) whose robust conductivity platoes representing different topological phases allowed to define with high precision a resistivity standard unit $R_K = \frac{h}{\varepsilon^2} = 25812.807557(18)\Omega$, hence having major impact in science and technology.

In the last two decades, a new type promising topological material has captivated the attention of many physicists. This is the Majorana wire, inspired in a famous Kitaev's toy model representing a spinless p-wave superconducting chain [1]. Under certain conditions, the Majorana wires experience topological phase transition characterized by the emergence of zero-modes localized at edges of the wire. Kitaev associated these modes with Majorana quasi-particles appearing at the boundary of the topological superconducting wires . Just like the IQHE, topology protects these Majorana's from quantum decoherence. In addition, Kitaev proposed that Majorana's non-abelian statistics provided a suitable method to encode quantum information [9]. These two characteristics gave the origin of an entire field called topological quantum computation [10].

The promise of using Majorana quasi-particles to implement quantum architectures motivated the pursuit of Majorana fermions during the following years. This motived a huge bunch of theoretical projects devoted to propose real implementations of the Kitaev model [2, 3, 11, 12**?** , 13]. The first experiment confirming the observation of Majorana zero modes (MZM) in topological superconductors was performed in 2012 by Mourik et al.. Since that moment, many other groups have created Majorana chains [15, 16, 17, 7, 18] These good experimental results inspired other ways to detect Majorana signatures. One of the most famous is the idea of coupling Majorana wires with QD's [4], which opened new lights to the design of quantum architectures with Majorana chains [19, 20].

In this chapter we will present a review of the main ideas behind the Kitaev chain (section section 3.1) and how that model inspired real implementations of Majorana wires section 3.2. In subsection 3.3.2 we will take a look to the idea of coupling QDs to a Majorana chain. This will be our last step before going into the main objective of this thesis: The manipulation of Majorana zero modes inside a double quantum dot.

3.1 The Kitaev Chain

Kitaev's tight binding toy model represents a finite p-wave superconducting wire with the following Hamiltonian

$$H = \sum_{i=1}^{N} \left[-t(a_i^\dagger a_{i+1} + a_{i+1}^\dagger a_i) - \mu a_i^\dagger a_i + \Delta a_i a_{i+1} + \Delta^* a_{i+1}^\dagger a_i^\dagger \right]. \tag{3.1}$$

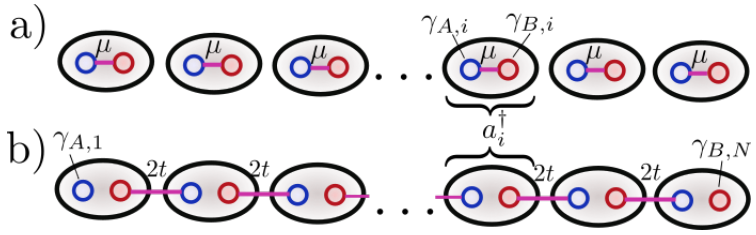

Figure 3.2: Illustration of the Kitaev chain for open boundary conditions in the Majorana representation. a)Represents the trivial case where the hopping and the superconducting term approaches to 0. b) The non-trivial topological phase. The coupling is produced between Majoranas in different Dirac fermions

Source: *By the author*

Where μ is the chemical potential, so that $\mu a_i^\dagger a_i$ is the energy associated to each step in the chain. $t(a_i^\dagger a_{i+1} + a_{i+1}^\dagger a_i)$ represents the interaction between neighboring sites which is determined by the hopping term t. The remaining terms describe the superconducting properties of the system as is is established by the BCS theory of superconductivity. Δ is a complex superconducting parameter with the form $\Delta = e^{i\theta}|\Delta|$. The associated terms represent the Cooper pairs which can be created or annihilated at neighboring sites of the system hence breaking particle number. However, the system still preserves parity, a property that will be very important during the rest of the project.

The form of Hamiltonian (Equation 3.1) favors the possibility of introducing new operators $\gamma_{A,j}$ and $\gamma_{B,j}$ such that

$$\gamma_{A,j} = e^{i\theta/2} a_j + e^{-i\theta/2} a_j^\dagger \ , \ \ \gamma_{B,j} = -i(e^{i\theta/2} a_j - e^{-i\theta/2} a_j^\dagger). \tag{3.2}$$

It is simple check that these operators are self-adjoint ($\gamma_{A,j}^\dagger = \gamma_{A,j}, \gamma_{A,j}^\dagger = \gamma_{B,j}$). This is a required constraint for the Majorana particles. In addition they satisfy the fermionic anti-commutation relations

$$\begin{aligned} \{\gamma_{A,i}, \gamma_{A,j}\} = \{\gamma_{B,i}, \gamma_{B,j}\} = 2\delta_{ij}, \\ \{\gamma_{A,i}, \gamma_{B,j}\} = 0. \end{aligned} \tag{3.3}$$

This allows us to understand the operators $\gamma_{A,i}, \gamma_{B,i}$ as Majorana fermions. If we also take the inverse of Equation 3.2 we obtain that each (Dirac) fermion in Hamiltonian (Equation 3.1) is composed by two Majorana fermions such that

$$a_j = \frac{e^{-i\theta/2}}{2}(\gamma_{A,j} + i\gamma_{B,j})$$

We could even adventure to say that these Majorana operators are actually dividing the Dirac fermions into real($\gamma_{A,}$) and imaginary ($\gamma_{B,}$) part ,the same way as complex numbers are a composite of two real numbers.

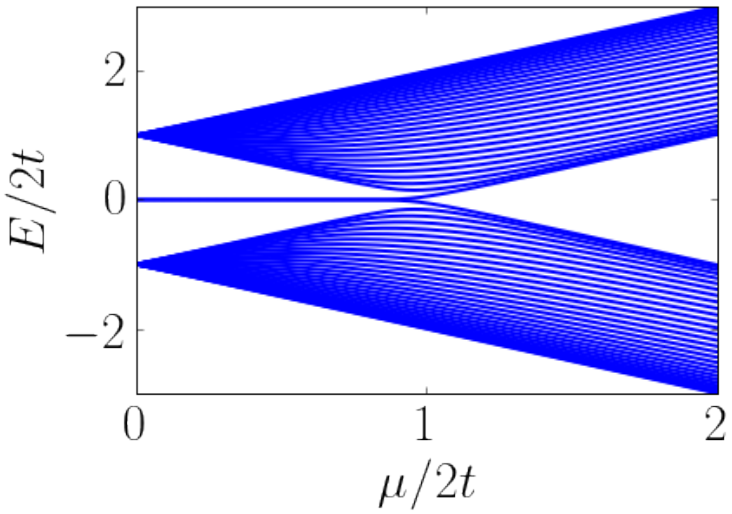

Figure 3.3: Spectrum of Hamiltonian Equation 3.4 with 30 sites and $t = |\Delta|$ s. Method: Numerical diagonalization.
Source: *By the author*

The new Kitaev Hamiltonian in the Majorana representation looks like

$$H = \frac{i}{2}\sum_{j=1}^{N}[-\mu\gamma_{A,j}\gamma_{B,j} + (t+|\Delta|)\gamma_{B,j}\gamma_{A,j+1} + (t-|\Delta|)\gamma_{A,j}\gamma_{B,j+1}] + Const, \tag{3.4}$$

Depending on the values of parameters μ, t and $|\Delta|$ we can identify two regimes represented by the following situations:

1. If $|\Delta| = t = 0$ and $\mu < 0$, Hamiltonian (Equation 3.4) becomes $\frac{-i\mu}{2}\sum_j \gamma_{A,j}\gamma_{B,j}$ which represents the coupling of the Majoranas in the same Dirac fermion. (See Figure 3.2 (a))

2. If $|\Delta| = t > 0$ and $\mu = 0$, the situation is much more interesting. The Hamiltonian (Equation 3.4) takes the form $H = 2ti\sum_j \gamma_{B,j}\gamma_{A,j+1}$. This implies that the coupling is performed between Majoranas of different Dirac fermions leaving the edge Majorana operators ($\gamma_{A,1}$ and $\gamma_{B,N}$) uncoupled (See Figure Figure 3.2b)). Note that these uncoupled Majorana fermions can be at any state without any repercussion in the energy of the system. This explains the emergence of a ground state localized at edges of the chain.

These two situations are representatives of two different phases. The trivial phase occurs for $\frac{\mu}{2t} > 1$ and the non-trivial phase appears when $\frac{\mu}{2t} < 1$ (See Figure 3.3). The mean characteristic of the non-trivial phase is the creation of an stable zero-mode generated by the uncoupled

Majorana fermions at the edges of the Kitaev chain. Note that if

$$H = 2ti\sum_{j}\gamma_{B,j}\gamma_{A,j+1}, \tag{3.5}$$

it is possible to define new Dirac fermion operators as

$$c_j = \frac{1}{\sqrt{2}}\left(\gamma_{B,j} + i\gamma_{A,j+1}\right)\ ,\ c_j^\dagger = \frac{1}{\sqrt{2}}\left(\gamma_{B,j} - i\gamma_{A,j+1}\right).$$

Then (Equation 3.6) becomes

$$H = ti\sum_{j=1}^{N-1}\left(2c_j^\dagger c_j - 1\right). \tag{3.6}$$

Then a ground state $|\Omega\rangle$ of this Hamiltonian is an state vacuum at all sites j from 1 to $N-1$ ($c_j|\Omega\rangle = 0$). This condition allows some degeneracy since the sites at the boundary are not coupled to the Hamiltonian $\gamma_{A,1}$ and $\gamma_{B,N}$. The Dirac operators formed by these Majoranas

$$c_N = \frac{1}{\sqrt{2}}\left(\gamma_{B,N} + i\gamma_{A,1}\right)\ ,\ c_N^\dagger = \frac{1}{\sqrt{2}}\left(\gamma_{B,N} - i\gamma_{A,1}\right),$$

can be either occupied ($c_N^\dagger c_N|\Omega\rangle = 1$) or empty ($c_N^\dagger c_N|\Omega\rangle = 0$). Each of these results will have a different parity that is a preserved symmetry of our Hamiltonian. Indeed we can define a global parity operator as

$$\mathscr{P} = \prod_{i=1}^{N}\left(c_j^\dagger c_j - 2\right) = \prod_{i=1}^{N} -i\gamma_{B,j}\gamma_{A,j+1} = \pm 1. \tag{3.7}$$

In the ground state $|\Omega\rangle$, this parity will be defined by the result of $\gamma_{B,N}\gamma_{A,1}$ since the other states are fix. This is a very important point, since this symmetry protection is actually correlating the two opposite sites of the Kitaev chain .i.e. Any attempt to disturb one site of the chain would have to change something on the other site, since the parity of the system must be preserved. This is a great deal, actually, it means that the coherence of Majorana fermions is actually very high. Why?. Then answer is topology and will be the objective of the next subsection.

3.1.1 Topological phase transition

The two regimes described previously can be characterized with a topological parameter. One of the methods for this is following the idea used by Alicea[3]. The first part is to suppose that we have an infinite chain ($N = \infty$) in Hamiltonian (Equation 3.4). The new system is translation invariant, hence we can make a transformation to the momentum space. Then we may rewrite Hamiltonian (Equation 3.4) as

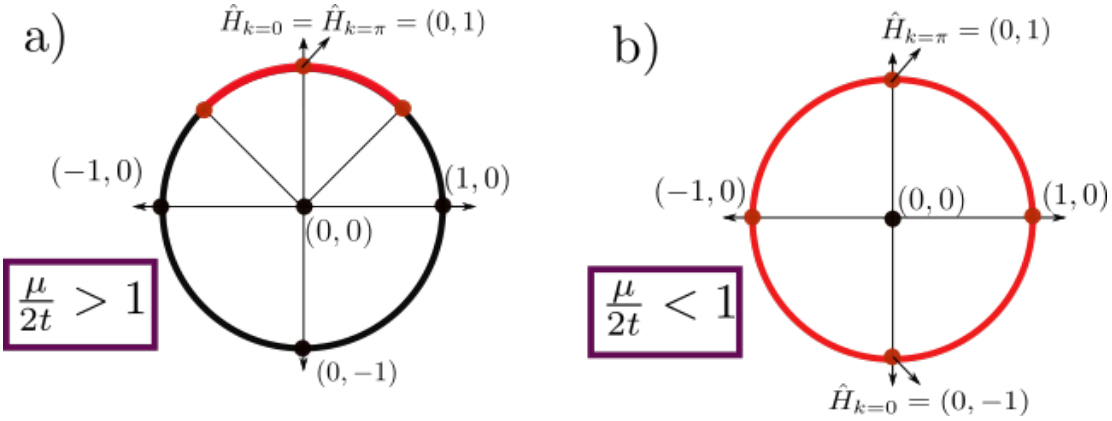

Figure 3.4: The following represents the path of $\hat{H}_k$ for the interval $[-\pi,\pi]$. a) Corresponds to the trivial phase. The resulting path can be homotopically deformed to a point. b) The non-trivial phase corresponds to a non-contractible loop around the unitary circle.
Source: *By the author*

$$H = \sum_{k\in BZ} \begin{pmatrix} b'_k & c'_k \end{pmatrix} H_k \begin{pmatrix} b'_{-k} \\ c'_{-k} \end{pmatrix}, \tag{3.8}$$

with the Bloch Hamiltonian equal to

$$H_k = \begin{pmatrix} 0 & \frac{-i\mu}{2} + it\cos k + |\Delta|\sin k \\ \frac{i\mu}{2} - it\cos k + |\Delta|\sin k & 0 \end{pmatrix} = (|\Delta|\sin k)\sigma_x + (\frac{\mu}{2} - t\cos k)\sigma_y. \tag{3.9}$$

Here, σ_x and σ_y are the corresponding Pauli matrices. The Brilloin zone (BZ) is the periodic space $[-\pi,\pi]$ which can be mapped to the unitary circle. Equation (Equation 3.9) determines the coordinates of the Bloch Hamiltonian in the base $\{\sigma_x,\sigma_y\}$.

We can map these coordinates to the unitary circle by taking the norm of this vector giving

$$\hat{H}_k = \frac{1}{\sqrt{|\Delta|^2\sin^2 k + (\frac{\mu}{2} - t\cos k)^2}} \begin{pmatrix} |\Delta|\sin k \\ \frac{\mu}{2} - t\cos k \end{pmatrix}. \tag{3.10}$$

Note that $|\Delta|^2\sin^2 k + (\frac{\mu}{2} - t\cos k)^2 \neq 0$ for all the values of k as long as $\frac{\mu}{2t} \neq 1$. When $\frac{\mu}{2t} = 1$ the $H_{k=0} = 0$, so it cannot be normalized. **This is the same point were the phase transition occurs!**. At any other value of $\frac{\mu}{2t}$ it is possible to normalize H_k for all values of $k \in BZ$. The result of mapping $\hat{H}_k$ for all k is a path around the unitary circle.

This path can take two forms as we can observe in Figure subsection 3.1.1. If $\frac{\mu}{2t} > 1$ the path reduced to a line in the upward part of the circle. In the non-trivial phase $\frac{\mu}{2t} < 1$ the path completes the round to the entire circle. Note that this method states a topological difference between the two phases. While the path described by the trivial phase can be contracted to a single dot, the path described by the non-trivial one is a circle that cannot be contracted.

Note that to determine whether path of a given phase is of type a) or type b) we only need to check if $\hat{H}_{k=0}$ and $\hat{H}_{k=\pi}$ are the same point or opposite points. This transforms into a simple equation

$$\hat{H}_{k=0,y}\hat{H}_{k=\pi,y} = \begin{cases} 1 & \text{trivial phase} \\ -1 & \text{non-trivial phase} \end{cases} \tag{3.11}$$

where $\hat{H}_{k=0,y}$ is the y-th component of $\hat{H}_k$. The term $\hat{H}_{k,y}$ is a particular case of the Pfaffian $\mathscr{P}(k)$, which widely used as topological order in phase transitions involving Majorana fermions.

The mean idea behind this topological characterization relies in the adiabatic theorem. In simple words, the adiabatic theorem says that a slow evolution of a gaped Hamiltonian will produce a smooth evolution of its ordered eigenstates. i.g The order of the eigenstates remains unchanged.

A keyword in the previous definition is "gaped". As we can observe in F Figure 3.3 the phase transition occurs at $\frac{\mu}{2t} = 1$. This point is where the gap of the Hamiltonian closes. In periodic boundary conditions no Majorana zero modes will emerge since there are no edges in the system. Therefore, the states with zero energy for $\frac{\mu}{2t} < 1$ will not appear at this situation. We obtain that the gapless point $\frac{\mu}{2t} = 1$ divides two gapped regions. If we are to follow the adiabatic theorem, these two regions must be separated, hence meaning that no adiabatic evolution could lead from one region to the other since that would involve crossing through a gapless region where state exchange is allowed.

To summarize, gapless points are forbidden points of our Hamiltonians in the middle of an adiabatic evolution. This forbidden points can be thought as "holes" in the space of Hamiltonians, which generates spaces with non-trivial topologies.Since adiabatic evolutions can be understood as smooth evolutions of the Hamiltonian, the relation with topology is clear. Then characterizing the phase transitions in the Kitaev chain, as in similar robust materials, is mainly a topological problem. Therefore, phase transitions can be characterized by topological quantities such as Pfaffians, Chern numbers or Winding numbers, which are always integer values.

This brings an interesting question. If we have two connected topological materials, one characterized by the number 0 and the other by the number 1, then what should happen at the surface?. Indeed something very exciting happens at these boundaries and those are the edge states, Majorana fermions, and all interesting topological phenomena in condensed matter.

Finally, note that in a system that preserve symmetries, the space of Hamiltonians has more forbidden sites. Therefore, these systems have a different topological characterization and more importantly, topology protects these symmetries. This is the case of the Kitaev chain where the topological phase protects the parity of the symmetry under perturbations involving the two

opposed Majoranas at the edges. This endowed topological stability combined with Majorana's non-abelian statistics (next subsection) makes the Kitaev chain a promising platform for quantum computation.

3.1.2 Non-abelian statistics

Imagine that we want to exchange two Majorana fermions γ_1 and γ_2 [2]. This procedure can be performed with an adiabatic evolution of the Hamiltonian $H(t)$ that exchanges both operators while leaving the system invariant. Therefore, after a period T we require that

$$\begin{aligned} \gamma_1(T) &= \gamma_2(0) \\ \gamma_2(T) &= \gamma_1(0) \end{aligned} \tag{3.12}$$

while $(H(0) = H(T))$.

The adiabatic evolution is then represented by a unitary operator $U(t) = e^{-\frac{i}{\hbar}\int H(t)}$ and is applied according to Heisenberg's picture as

$$\gamma_i(T) = U^\dagger(t)\gamma_i(0)U(t).$$

Since Majoranas preserve fermion parity, H must commute with the parity operator $P = -i\gamma_1\gamma_2$. In a Clifford algebra generated by the operators γ_1 and γ_2 (See algebraic relations (Equation 3.3)), $[H, \gamma_1\gamma_2] = 0$ implies that $H(t) \propto \gamma_1\gamma_2$ or $H(t)$ is a constant. Taking the non-trivial answer we obtain that the evolution operator has the form $U(t) = e^{\alpha(t)\gamma_1\gamma_2}$, where $\alpha(t)$ is a complex function over t. We can simplify this exponential noting that $(\gamma_1\gamma_2)^2 = -1$ which after Taylor expansion reduces to

$$U(t) = \cos(\alpha(t)) - \gamma_1\gamma_2\sin(\alpha(t)). \tag{3.13}$$

Replacing this solution in (Equation 3.12) we obtain

$$\begin{aligned} \gamma_1(T) &= \gamma_1\cos(2\alpha(T)) - \gamma_2\sin(2\alpha(T)) = \gamma_2 \\ \gamma_2(T) &= \gamma_2\cos(2\alpha(T)) + \gamma_1\sin(2\alpha(T)) = \gamma_1, \end{aligned} \tag{3.14}$$

which can only happen if $\alpha(T) = \pm\frac{\pi}{4}$. Hence we conclude that the exchange operator between both Majoranas is

$$U_{12} = e^{\pm\frac{\pi}{4}\gamma_1\gamma_2} = \frac{1}{\sqrt{2}}(1 \pm \gamma_1\gamma_2). \tag{3.15}$$

Note that this exchange does not depend on the evolution, nor the period of time.

Now imagine that we have three Majoranas γ_1, γ_2 and γ_3 and we want to perform the following processes. On the first one, we exchange Majoranas 1 and 2 and then the Majorana in 2 (which was initially at 1) is exchanged with Majorana 3 (Figure 3.5[Left]). On the second

[2] This section is inspired on the page topocondmat `https://topocondmat.org/w2_majorana/braiding.html`, which contains an amazing tutorial about Majorana fermions and topological insulators.

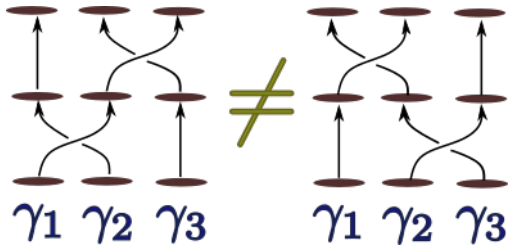

Figure 3.5: Representation of non-abelian braiding .

process, we invert the order, hence exchanging first exchange Majoranas 2 and 3 and then Majoranas 1 and 2 (Figure 3.5[Right]). These two cases are represented by the following operators respectively

$$\begin{aligned} U_{23}U_{12} &= \frac{1}{2}(1+\gamma_2\gamma_3)(1+\gamma_1\gamma_2) = \frac{1}{2}(1+\gamma_2\gamma_3+\gamma_1\gamma_2+\gamma_3\gamma_1) \\ U_{12}U_{23} &= \frac{1}{2}(1+\gamma_1\gamma_2)(1+\gamma_2\gamma_3) = \frac{1}{2}(1+\gamma_1\gamma_2+\gamma_2\gamma_3+\gamma_1\gamma_3)\,. \end{aligned} \tag{3.16}$$

Since $\gamma_3\gamma_1 = -\gamma_1\gamma_3$, the outcome of both processes is essentially different, which means that it actually matters the order in which the Majoranas are exchanged .

The particles that satisfy this strange property receive the name of non-abelian anyons. While the word "anyon" usually integrates several types of particles including bosons and fermions, the word non-abelian emphasis on the non-commutative exchange statistics.

Non-abelian statistics is what make anyons a fantastic candidate to implement quantum algorithms. The idea of exchanging anyons can be thought as a braiding like in Figure 3.5. Since the order of braiding matters, different braiding orders can be associated to distinct algorithms. This generates another form of codifying information which has been extendedly studied in knot theory [21]. And if these anyons where topological, they will be protected from quantum decoherence [22]. To the date, the closest candidates to satisfy both properties (non-abelian statistics, topological characterization) are the Majorana fermions. Notwithstanding, the basic braiding protocol that would unleash the keys to topological quantum computation [10] has not been measured yet. Many theoretical proposals have been set up in this direction, but there is still a long experimental road.

3.2 Real implementations of the Kitaev Chain

One of the main problems to implement real devices capable to exhibit Majorana quasi-particles at the boundaries, was that Majorana's are spin-less. Since all materials have fermion doubling, it was necessary to endow the system with a physical property that could separate the spin energy bands. To bypass this problem, Lutchyn et al. proposed using a material with strong

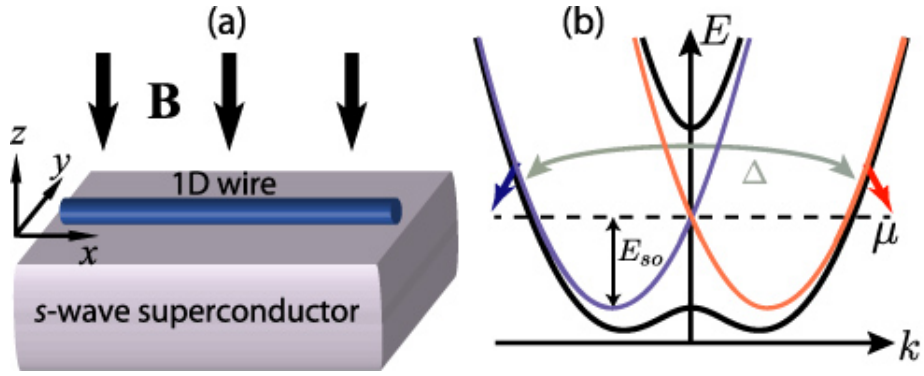

Figure 3.6: Source: *[3]*

spin-orbit Rashba interaction [24], which would split the energy band by spin, hence destroying fermion doubling.

This idea allowed scientist to designed the first Majorana wires. The recipe consists ingrowing a semi-conducting wire with high spin-orbit coupling, over an s'wave superconductor and inducing a Zeeman magnetic field (Figure 3.6(a)). Such model is described by the following Hamiltonian [3](65)

$$H = \int \mathrm{d}x \psi^\dagger \left(\frac{-1}{2m}\partial_x^2 - \mu - i\alpha\sigma_y\partial_x + h\sigma_x \right) \psi + \Delta\psi_\downarrow\psi_\uparrow + \Delta^*\psi_\downarrow\psi_\uparrow, \tag{3.17}$$

where μ is the chemical potential, h is the Zeeman splitting energy, Δ is the superconducting gap and $\alpha > 0$ is the Rashba spin-coupling parameter, favoring spin-align. If $\Delta = 0$, the band structure would split and divide in two bands [3](67)

$$\varepsilon_\pm(k) = \frac{k^2}{2m} - \mu \pm \sqrt{(\alpha k)^2 + h^2} \tag{3.18}$$

with opposed spins as observed in the blue and red lines of Figure 3.6(b).

The superconducting proximity effect opens a gap Δ that projects the upper and lower bands forming as observe in the black bands of Figure 3.6(b) . The separation of both energy channels allow us to think the conduction band as an spin-less system where Majorana modes can emerge. As pointed out by Alicea, the system is in the topological phase if the the following criterion is satisfied

$$h > \sqrt{\Delta^2 + \mu^2}. \tag{3.19}$$

This theoretical proposal led in 2012 to the first observation of Majorana signatures in InSb nanowires [3], by Mourik et al. from the Kavli Institute at Delft. This was a huge boost to the field which immediately attracted abundant experimental and theoretical work.

[3] A material with strong spin-orbit coupling and large g factor.

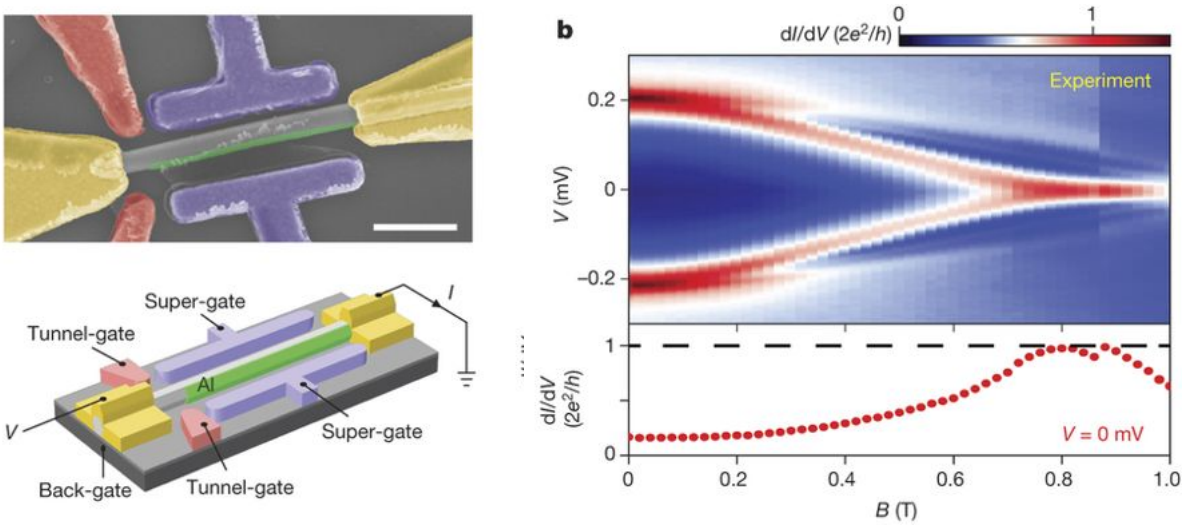

(a) (b)

Figure 3.7: (a) Experimental setup (b) Observed magnetic field dependance of the zero bias peak.
Source: *[18]*

In just 6 years, more than 5 groups have documented the observation of Majorana signatures [15, 16, 17, 7, 18]. This signature is characterized by the emergence of a robust zero bias conductance peak ZBCP of height $\frac{2e^2}{\hbar}$ produced by the Majorana zero mode MZM localized at the edges of the wire. Though the first experiments didn't observed such an stable signature, the last year Zhang et al. published a paper documenting the observation of this robust peak with the expected theoretical magnitude in and InSb wire Figure 3.7. As can be observed in Figure 3.7(b) the ZBCP increases up to $\frac{2e^2}{\hbar}$ for a strong magnetic field, where the system enters the topological phase according to equation (Equation 3.19).

Despite the successful experimental results, there is still certain skepticism about the existence of Majorana fermions mainly, because Majorana zero-modes (MZM) have been found in superposition with other similar types of phenomenon such Andreev bound states or even the Kondo effect. [25] The new experimental proposals focus on distinguishing MZMs from other effects and implementing braiding protocols [13, 12**?**] . One promising idea that could lead to important results in both research lines is coupling Majorana wires with QDs. This will be the objective of the following section.

3.3 Coupling Majorana Fermions to QDs

Liu and Baranger were the first to propose the possibility of using QDs in the pursuit of Majo-

rana fermions . When a QD is attached to the end of a Majorana chain in the topological phase, the Majorana Zero Mode at the end of the chain leaks inside the QD [6] producing a zero-bias conductance peak of half a quanta $\frac{e^2}{2h}$ through the dot. This method of detecting Majorana signatures presents the following advantages:

1. The qubit information is not completely destroyed, in contrast to other detection methods such as tunneling spectroscopy.

2. If performed under the Kondo temperature T_k it allows the possibility of observing the MZM co-existing with the Kondo peak, [5, 8, 26] .

3. Today's precise experimental control over the QD parameters allows the manipulation of MZMs inside multi-dot systems, which offers new possibilities to design of quantum architectures with Majorana chains.[19, 20]

In this project we will main exploit the second and the third hints to manipulate MZMs in double quantum dot systems. But before going through that model it is necessary to understand the single dot-Majorana coupling.

3.3.1 Model

In this section we will recreate the results of Liu and Baranger using the methods developed in **??** . This will also allow us to probe our methods in a system with Majorana zero modes.

The Hamiltonian for Majorana-QD-lead hybrid system is given by

$$H = H_{QD-Lead} + H_{M-QD} + H_M. \tag{3.20}$$

Where $H_{QD-Lead}$ is the Hamiltonian for the non-interacting Anderson model (**??**), H_M is the Hamiltonian of the Majorana chain and H_{M-QD} represents the coupling between the QD and the Majorana Fermion at the boundary.

Now, the real question is how to define the coupling between the QD and the Majorana fermion. In fact, there are many ways to represent this interaction. One alternative is to replace in H_M with the entire Kitaev chain hamiltonian (Equation 3.1) (or even with the Majorana chain (Equation 3.17)) and then pick H_{M-QD} as a simple coupling between the QD and the first site of the chain [6]. A simpler approach is to define an effective coupling with the Majorana operator at the edge of the Majorana chain. Since the Kitaev chain is spin-less, we choose to couple the Majorana to the spin-$\downarrow$ channel of the QD [4] . Therefore, the Majorana fermion should be the superposition of the creation and annihilation operators of a spin $\downarrow$ particle $f_\downarrow$:

$$\gamma_1 := \frac{1}{\sqrt{2}}\left(f_\downarrow^\dagger + f_\downarrow\right), \gamma_2 := \frac{1}{\sqrt{2}}\left(f_\downarrow^\dagger - f_\downarrow\right).$$

[4] An appropriate justification of this fact can be found in [8]

This makes possible to define an effective coupling between the Majorana Mode and the dot by attaching γ_1 with the spin-$\downarrow$ channel in the QD

$$H_{M-QD} = t_1\left(d_\downarrow^\dagger\gamma_1+\gamma_1 d_\downarrow\right) \tag{3.21}$$

Then the coupling with the chain is given by

$$\begin{aligned} H_M &= \varepsilon_m f_\downarrow^\dagger f_\downarrow \\ H_{M-QD} &= \frac{t_1}{\sqrt{2}}d_{1\downarrow}^\dagger f_\downarrow+\frac{t_1^*}{\sqrt{2}}f_\downarrow^\dagger d_{1\downarrow}+\frac{t_1}{\sqrt{2}}d_{1\downarrow}^\dagger f_\downarrow^\dagger+\frac{t_1^*}{\sqrt{2}}f_\downarrow d_{1\downarrow} \end{aligned}$$

Finally we obtain the following hamiltonian

$$H=\sum_{k,\sigma}\left(\varepsilon_1+\frac{U_1}{2}\right)d_{1\sigma}^\dagger d_{1\sigma}+\frac{U}{2}(d_{1\sigma}^\dagger d_{1\sigma}-1)^2+t_1\left(d_{1\downarrow}^\dagger\gamma_1+\gamma_1 d_{1\downarrow}\right)+Vd_{1\sigma}^\dagger c_{k\sigma}+V^*c_{k\sigma}^\dagger d_{1\sigma}+\varepsilon_m f_\downarrow^\dagger f_\downarrow. \tag{3.22}$$

The fidelity of this effective model has been discussed by Ruiz-Tijerina et al. [8] concluding that this model reproduces the same results than coupling a Kitaev chain model in the topological phase to a QD. (This statement is true even for more realistic models of the TS including Rashba spin-orbit interactions and a Zeeman field [8]).

3.3.2 Non-interacting QD coupled to Majorana chain

In the non-interacting case we can use the ballistic transport equations from **??**.The green functions are then determined by the following set of linear equations.

$$(\omega-\varepsilon_M)\,G_{f_\downarrow,d_{1\downarrow}^\dagger}(\omega)=(\omega+\varepsilon_M)\,G_{f_\downarrow^\dagger,d_{1\downarrow}^\dagger}(\omega)=\frac{t_1^*}{\sqrt{2}}\left(G_{d_{1\downarrow},d_{1\downarrow}^\dagger}(\omega)-G_{d_{1\downarrow}^\dagger,d_{1\downarrow}^\dagger}(\omega)\right) \tag{3.23}$$

$$(\omega-\varepsilon_1)\,G_{d_{1\downarrow},d_{1\downarrow}^\dagger}(\omega)=1+\frac{t_1}{\sqrt{2}}t_1G_{f_\downarrow,d_{1\downarrow}^\dagger}(\omega)+\frac{t_1}{\sqrt{2}}t_1G_{f_\downarrow^\dagger,d_{1\downarrow}^\dagger}(\omega)+V_1\sum_{\mathbf{k}}G_{c_{\mathbf{k}\downarrow},d_{1\downarrow}^\dagger}(\omega) \tag{3.24}$$

$$(\omega-\varepsilon_{\mathbf{k}})\,G_{c_{\mathbf{k}},d_{1\downarrow}^\dagger}(\omega)=V_1^*G_{d_{1\downarrow},d_{1\downarrow}^\dagger}(\omega) \tag{3.25}$$

$$(\omega+\varepsilon_1)\,G_{d_{1\downarrow}^\dagger,d_{1\downarrow}^\dagger}(\omega)=-\frac{t_1}{\sqrt{2}}G_{f_\downarrow,d_{1\downarrow}^\dagger}(\omega)-\frac{t_1}{\sqrt{2}}G_{f_\downarrow^\dagger,d_{1\downarrow}^\dagger}(\omega)-V_1^*\sum_{\mathbf{k}}G_{c_{\mathbf{k}\downarrow}^\dagger,d_{1\downarrow}^\dagger}(\omega) \tag{3.26}$$

$$(\omega+\varepsilon_{\mathbf{k}})\,G_{c_{\mathbf{k}}^\dagger,d_{1\downarrow}^\dagger}(\omega)=-V_1^*G_{d_{1\downarrow},d_{1\downarrow}^\dagger}(\omega) \tag{3.27}$$

The graph representing these green functions is represented in Figure 3.8 a) (Look **??** for details). However using that $(\omega-\varepsilon_M)\,G_{f_\downarrow,d_{1\downarrow}^\dagger}(\omega)=(\omega+\varepsilon_M)\,G_{f_\downarrow^\dagger,d_{1\downarrow}^\dagger}(\omega)$ we can take $G_{f_\downarrow^\dagger,d_{1\downarrow}^\dagger}(\omega)$ out of the equations. After eliminating this term Equation 3.24 becomes

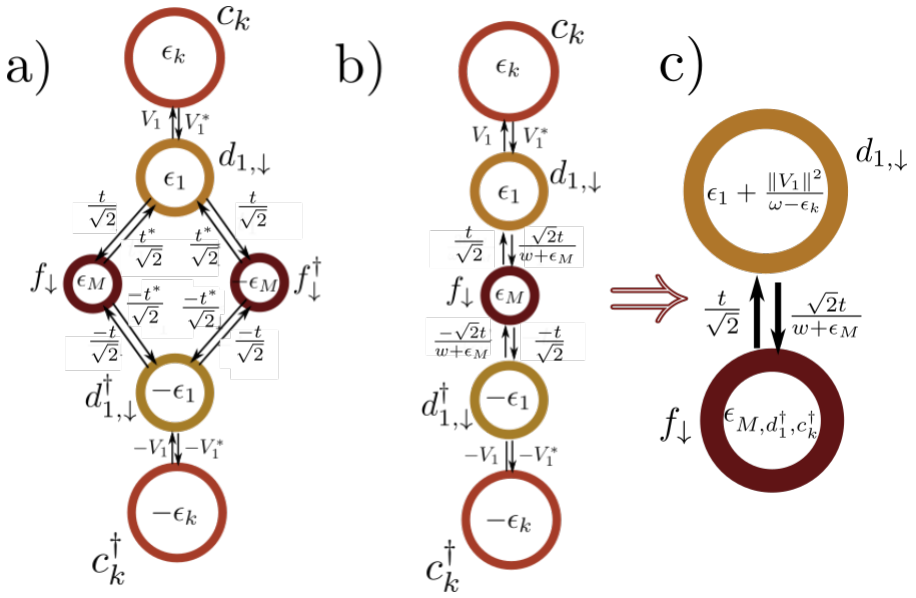

Figure 3.8: Graph $\mathscr{G}_M$ representing the transport equations. Source: *By the author*

$$(\omega-\varepsilon_1)\,G_{d_{1\downarrow},d_{1\downarrow}^\dagger}(\omega) = 1+\frac{t_1}{\sqrt{2}}\left(1+\frac{\omega-\varepsilon_M}{\omega+\varepsilon_M}\right)G_{f_\downarrow,d_{1\downarrow}^\dagger}(\omega)+V_1\sum_{\mathbf{k}}G_{c_{\mathbf{k}\downarrow},d_{1\downarrow}^\dagger}(\omega) \tag{3.28}$$

$$= 1+\frac{\sqrt{2}t_1}{\omega+\varepsilon_M}G_{f_\downarrow,d_{1\downarrow}^\dagger}(\omega)+V_1\sum_{\mathbf{k}}G_{c_{\mathbf{k}\downarrow},d_{1\downarrow}^\dagger}(\omega) \tag{3.29}$$

Similarly,

$$(\omega+\varepsilon_1)\,G_{d_{1\downarrow}^\dagger,d_{1\downarrow}^\dagger}(\omega) = -\frac{\sqrt{2}t_1}{\omega+\varepsilon_M}G_{f_\downarrow,d_{1\downarrow}^\dagger}(\omega)-V_1^*\sum_{\mathbf{k}}G_{c_{\mathbf{k}\downarrow}^\dagger,d_{1\downarrow}^\dagger}(\omega) \tag{3.30}$$

With these new equations we obtain new associated graph is in Figure 3.8 b) . Using the graph algorithm from **??** we proceed to pop out vertexes c_k , $c_k^\dagger$ and $d_1^\dagger$ in that order. The result is the graph in figure Figure 3.8.c) with

$$\varepsilon_{M,d_1^\dagger,c^\dagger} = \varepsilon_M+\frac{\omega}{\omega+\varepsilon_M}\frac{\|t\|^2}{\omega+\varepsilon_1+\sum_{\mathbf{k}}\frac{V_1V_1^*}{\omega+\varepsilon_{\mathbf{k}}}}. \tag{3.31}$$

We finally pop out $f_\downarrow$ to obtain

$$G_{d_{1\downarrow},d_{1\downarrow}^\dagger}(\omega) = \left[\omega-\varepsilon_1-\sum_{\mathbf{k}}\frac{V_1V_1^*}{\omega-\varepsilon_1}-\frac{\omega}{\omega+\varepsilon_M}\frac{\|t\|^2}{\omega-\varepsilon_{M,d_1^\dagger,c^\dagger}}\right]^{-1}. \tag{3.32}$$

This is the Green function we have been looking for. After a few algebraic operations it is possible to show that this result is equivalent to the first computation done by Liu and Baranger in the paper [4].

To compute the DOS we need to replace $\sum \frac{V_1 V_1^*}{\omega - \varepsilon_k} = -i\Gamma_1$ as we already did in **??**. Note that these computations are only for the spin-$\downarrow$ channel. The spin-$\uparrow$ channel is even simpler since this channel is not coupled to the Majorana mode by convention. Hence it corresponds to the case of a single quantum dot coupled to a Lead. The results for the DOS can be observed in Figure 3.9. Each figure has an inset showing the model in the Majorana representation. The small blue and red balls are Majorana fermions just as the ones in figure Figure 3.2. The Majorana at the edge of the chain is represented by the isolated red ball connected to the QD (Figure 3.9a). The other isolated blue ball in Figure 3.9c represents the Majorana at the other edge which is connected to the sphere by the parameter ε.

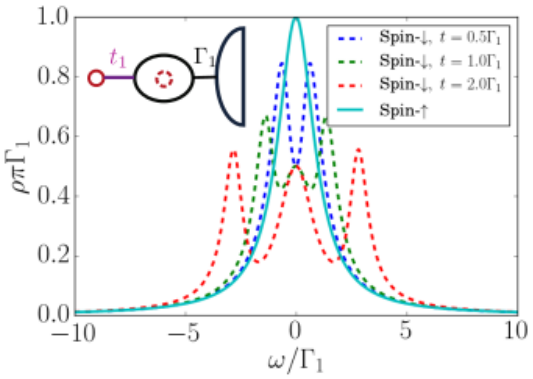

(a) Tuning the Majorana coupling t_1

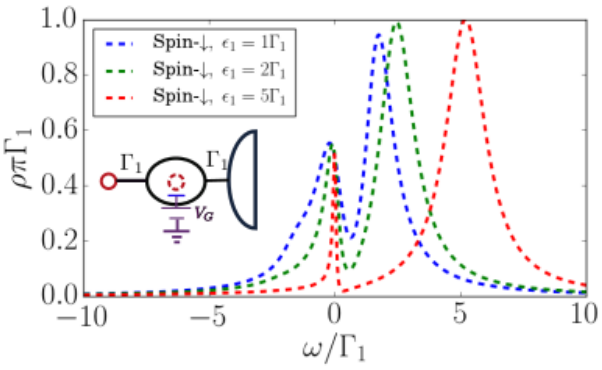

(b) Tuning dot's gate voltage ε_1

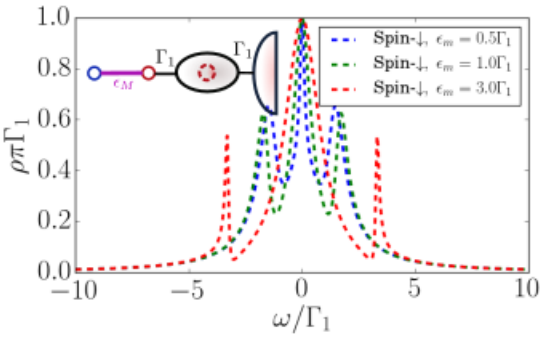

(c) Tuning ε_M

Figure 3.9: Density of states for a Majorana coupled to a QD under the tuning of different parameter. The tuning parameter is drawn in purple line in the inset model.

Source: *By the author*

- **Figure 3.9.(a),(b):** The spin-↑ DOS shows the result of coupling the QD with the lead and without Majorana fermions. When the parameter t is increased, the Majorana fermion is couple to the spin-↓ which causes the dispersion of the DOS. The most relevant signature is the robust height of 0.5 in the DOS that is observed in the central peak for all $t > 0$. This mid-height DOS is responsible for the decay of half a quanta in the conductivity of the QD.

- **Figure 3.9.(c),(d):** This time a gate voltage is induced in the dot which breaks PHS. However the robust 0.5-height Majorana signature prevails in the dot even at very high gate voltages where the dot is expected to be empty.

- **Figure 3.9.(e),(f):** The term ε_M couples both Majoranas at the edges of the chain. The strength of this parameter decays exponentially with the length of the Majorana chain so that it is often neglected . Here we observe the consequences of including this parameter in the model. The spin-↓ DOS emulates the spin-↑ DOS for energies $\omega < \varepsilon_M$. This clearly destroys the Majorana zero mode.

3.3.3 Kondo-Majorana physics

In interacting quantum dots the Kondo effect is visible at low temperatures even when the QD is attached to a Majorana chain, hence allowing us to study the combined Kondo-Majorana physics. To observe this effect, we used the NRG code with a fixed Coulomb repulsion of $U = 17\Gamma_1$ just as in section **??**. Thus, particle-hole equilibrium is achieved when $\left(\varepsilon_1 + \frac{U_1}{2}\right)\hat{n}_{1\sigma}$. Figure 3.10 shows this case. The spin-↑ DOS emulates the Kondo peak from Figure **??**. The spin-↓ DOS instead, reveals a Majorana zero mode of half the amplitude of the Kondo peak. This new type of Majorana signature resembles the one in Figure 3.9a. However, the energy scale where this physics is observed is one order of magnitude less than in the non-interacting case.

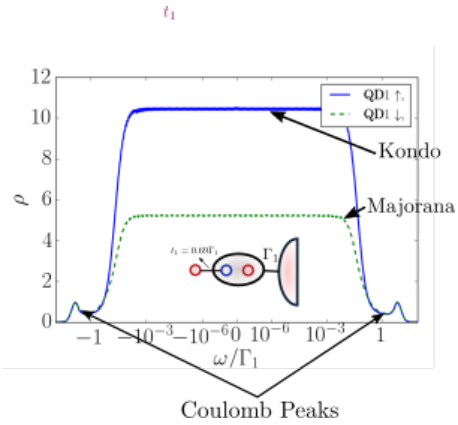

Figure 3.10: Note *The units of this plot are a bit different than the NRG plots. That's mainly due to a problem I am having with the NRG plots. I will unify the format soon.*
Source: *[?]*

Ruiz-Tijerina et al. proved that this effective coupling is able to reproduce efficiently the results obtained when the Kitaev chain in the topological phase is attached to a single QD.

Bibliography

[1] A. Yu Kitaev. Unpaired Majorana fermions in quantum wires. *Phys.-Usp.*, 44(10S):131, 2001. ISSN 1063-7869. doi: 10.1070/1063-7869/44/10S/S29. URL http://stacks.iop.org/1063-7869/44/i=10S/a=S29. 1, 3

[2] Jason Alicea. Majorana fermions in a tunable semiconductor device. *Phys. Rev. B*, 81 (12):125318, March 2010. doi: 10.1103/PhysRevB.81.125318. URL https://link.aps.org/doi/10.1103/PhysRevB.81.125318. 1, 3

[3] Jason Alicea. New directions in the pursuit of Majorana fermions in solid state systems. *Rep. Prog. Phys.*, 75(7):076501, 2012. ISSN 0034-4885. doi: 10.1088/0034-4885/75/7/076501. URL http://stacks.iop.org/0034-4885/75/i=7/a=076501. 1, 3, 3.1.1, 3.6, 3.2, 3.2, 3.2

[4] Dong E. Liu and Harold U. Baranger. Detecting a majorana-fermion zero mode using a quantum dot. 84(20). ISSN 1098-0121, 1550-235X. doi: 10.1103/PhysRevB.84.201308. URL http://arxiv.org/abs/1107.4338. 1, 3, 3.3, 3.3.1, 3.3.2

[5] Minchul Lee, Jong Soo Lim, and Rosa Lopez. Kondo effect in a quantum dot side-coupled to a topological superconductor. 87(24):241402. doi: 10.1103/PhysRevB.87.241402. URL https://link.aps.org/doi/10.1103/PhysRevB.87.241402. 1, 2

[6] E. Vernek, P. H. Penteado, A. C. Seridonio, and J. C. Egues. Subtle leakage of a majorana mode into a quantum dot. 89(16):165314. doi: 10.1103/PhysRevB.89.165314. URL https://link.aps.org/doi/10.1103/PhysRevB.89.165314. 1, 3.3, 3.3.1

[7] M. T. Deng, S. Vaitiekenas, E. B. Hansen, J. Danon, M. Leijnse, K. Flensberg, J. Nygard, P. Krogstrup, and C. M. Marcus. Majorana bound state in a coupled quantum-dot hybrid-nanowire system. 354(6319):1557–1562. ISSN 0036-8075, 1095-9203. doi: 10.1126/science.aaf3961. URL http://science.sciencemag.org/content/354/6319/1557. 1, 3, 3.2

[8] David A. Ruiz-Tijerina, E. Vernek, Luis G. G. V. Dias da Silva, and J. C. Egues. Interaction effects on a majorana zero mode leaking into a quantum dot. 91(11):115435. doi: 10.1103/PhysRevB.91.115435. URL https://link.aps.org/doi/10.1103/PhysRevB.91.115435. 1, 2, 4, 3.3.1, 3.3.3

[9] A. Yu Kitaev. Fault-tolerant quantum computation by anyons. *Annals of Physics*, 303 (1):2–30, January 2003. ISSN 00034916. doi: 10.1016/S0003-4916(02)00018-0. URL http://arxiv.org/abs/quant-ph/9707021. arXiv: quant-ph/9707021. 3

[10] Jiannis K. Pachos. *Introduction to Topological Quantum Computation*. Cambridge University Press, Cambridge ; New York, 1 edition edition, May 2012. ISBN 978-1-107-00504-4. 3, 3.1.2

[11] C.w.j. Beenakker. Search for Majorana Fermions in Superconductors. *Annual Review of Condensed Matter Physics*, 4(1):113–136, March 2013. ISSN 1947-5454. doi: 10.1146/annurev-conmatphys-030212-184337. URL https://www.annualreviews.org/doi/10.1146/annurev-conmatphys-030212-184337. 3

[12] Sankar Das Sarma, Michael Freedman, and Chetan Nayak. Majorana zero modes and topological quantum computation. *npj Quantum Information*, 1:15001, October 2015. ISSN 2056-6387. doi: 10.1038/npjqi.2015.1. URL https://www.nature.com/articles/npjqi20151. 3, 3.2

[13] David Aasen, Michael Hell, Ryan V. Mishmash, Andrew Higginbotham, Jeroen Danon, Martin Leijnse, Thomas S. Jespersen, Joshua A. Folk, Charles M. Marcus, Karsten Flensberg, and Jason Alicea. Milestones Toward Majorana-Based Quantum Computing. *Physical Review X*, 6(3):031016, August 2016. doi: 10.1103/PhysRevX.6.031016. URL https://link.aps.org/doi/10.1103/PhysRevX.6.031016. 3, 3.2

[14] V. Mourik, K. Zuo, S. M. Frolov, S. R. Plissard, E. P. a. M. Bakkers, and L. P. Kouwenhoven. Signatures of Majorana Fermions in Hybrid Superconductor-Semiconductor Nanowire Devices. *Science*, 336(6084):1003–1007, May 2012. ISSN 0036-8075, 1095-9203. doi: 10.1126/science.1222360. URL http://science-sciencemag-org.ez67.periodicos.capes.gov.br/content/336/6084/1003. 3, 3.2

[15] Anindya Das, Yuval Ronen, Yonatan Most, Yuval Oreg, Moty Heiblum, and Hadas Shtrikman. Zero-bias peaks and splitting in an Al-InAs nanowire topological superconductor as a signature of Majorana fermions. *Nature Physics*, 8(12):887, December 2012. ISSN 1745-2481. doi: 10.1038/nphys2479. URL https://www.nature.com/articles/nphys2479. 3, 3.2

[16] M. T. Deng, C. L. Yu, G. Y. Huang, M. Larsson, P. Caroff, and H. Q. Xu. Anomalous Zero-Bias Conductance Peak in a Nb-InSb Nanowire-Nb Hybrid Device. *Nano Letters*, 12(12):6414–6419, December 2012. ISSN 1530-6984. doi: 10.1021/nl303758w. URL http://dx.doi.org/10.1021/nl303758w. 3, 3.2

[17] Stevan Nadj-Perge, Ilya K. Drozdov, Jian Li, Hua Chen, Sangjun Jeon, Jungpil Seo, Allan H. MacDonald, B. Andrei Bernevig, and Ali Yazdani. Observation of Majorana

fermions in ferromagnetic atomic chains on a superconductor. *Science*, 346(6209):602–607, October 2014. ISSN 0036-8075, 1095-9203. doi: 10.1126/science.1259327. URL http://science.sciencemag.org/content/346/6209/602. 3, 3.2

[18] Hao Zhang, Chun-Xiao Liu, Sasa Gazibegovic, Di Xu, John A. Logan, Guanzhong Wang, Nick van Loo, Jouri D. S. Bommer, Michiel W. A. de Moor, Diana Car, Roy L. M. Op het Veld, Petrus J. van Veldhoven, Sebastian Koelling, Marcel A. Verheijen, Mihir Pendharkar, Daniel J. Pennachio, Borzoyeh Shojaei, Joon Sue Lee, Chris J. PalmstrÃžm, Erik P. A. M. Bakkers, S. Das Sarma, and Leo P. Kouwenhoven. Quantized Majorana conductance. *Nature*, 556:74, March 2018. URL http://dx.doi.org/10.1038/nature26142. 3, 3.7, 3.2

[19] Maissam Barkeshli and Jay D. Sau. Physical Architecture for a Universal Topological Quantum Computer based on a Network of Majorana Nanowires. *arXiv:1509.07135 [cond-mat, physics:quant-ph]*, September 2015. URL http://arxiv.org/abs/1509.07135. arXiv: 1509.07135. 3, 3

[20] Torsten Karzig, Christina Knapp, Roman M. Lutchyn, Parsa Bonderson, Matthew B. Hastings, Chetan Nayak, Jason Alicea, Karsten Flensberg, Stephan Plugge, Yuval Oreg, Charles M. Marcus, and Michael H. Freedman. Scalable designs for quasiparticle-poisoning-protected topological quantum computation with Majorana zero modes. *Physical Review B*, 95(23):235305, June 2017. doi: 10.1103/PhysRevB.95.235305. URL https://link.aps.org/doi/10.1103/PhysRevB.95.235305. 3, 3

[21] Vladimir G. Turaev. *Quantum Invariants of Knots and 3-Manifolds*. De Gruyter, Berlin, Boston, 3rd corr. ed. edition, 2016. ISBN 978-3-11-043522-1. URL https://www.degruyter.com/view/product/461906. 3.1.2

[22] Chetan Nayak, Steven H. Simon, Ady Stern, Michael Freedman, and Sankar Das Sarma. Non-Abelian anyons and topological quantum computation. *Reviews of Modern Physics*, 80(3):1083–1159, September 2008. doi: 10.1103/RevModPhys.80.1083. URL https://link.aps.org/doi/10.1103/RevModPhys.80.1083. 3.1.2

[23] Roman M. Lutchyn, Jay D. Sau, and S. Das Sarma. Majorana Fermions and a Topological Phase Transition in Semiconductor-Superconductor Heterostructures. *Physical Review Letters*, 105(7):077001, August 2010. doi: 10.1103/PhysRevLett.105.077001. URL https://link.aps.org/doi/10.1103/PhysRevLett.105.077001. 3.2

[24] A. Manchon, H. C. Koo, J. Nitta, S. M. Frolov, and R. A. Duine. New perspectives for Rashba spinâorbit coupling. *Nature Materials*, 14(9):871–882, September 2015. ISSN 1476-4660. doi: 10.1038/nmat4360. URL https://www.nature.com/articles/nmat4360. 3.2

[25] Eduardo J. H. Lee, Xiaocheng Jiang, RamÃ3*nAguado*, *GeorgiosKatsaros*, *Charles M.Lieber*, *andSilvanoDe Francesch* *BiasAnomalyinaNanowireQuantumDotCoupledtoSuperconductors.Physical Review Letters*, 109 (18) : 186802, *October*2012.*doi* : . URL https://link.aps.org/doi/10.1103/PhysRevLett.109.186802. 3.2

G. Górski, J. Barański, I. Weymann, and T. DomaÅski. Interplay between correlations and Majorana mode in proximitized quantum dot. *Scientific Reports*, 8(1):15717, October 2018. ISSN 2045-2322. 10.1038/s41598-018-33529-1. URL https://www.nature.com/articles/s41598-018-33529-1. 2

H. R. Krishna-murthy, J. W. Wilkins, and K. G. Wilson. Renormalization-group approach to the Anderson model of dilute magnetic alloys. 1. Static properties for the symmetric case. *Phys.Rev.*, B21:1003–1043, 1980. 10.1103/PhysRevB.21.1003. A.1, A.1

Michael Sindel. *Numerical Renormalization Group studies of Quantum Impurity Models in the Strong Coupling Limit*. Text.PhDThesis, Ludwig-Maximilians-UniversitÃt MÃŒnchen, January 2005. URL https://edoc.ub.uni-muenchen.de/3115/. A.1

Ralf Bulla, Theo A. Costi, and Thomas Pruschke. Numerical renormalization group method for quantum impurity systems. *Reviews of Modern Physics*, 80(2):395–450, April 2008. 10.1103/RevModPhys.80.395. URL https://link.aps.org/doi/10.1103/RevModPhys.80.395. A.1

M. A. Ruderman and C. Kittel. Indirect Exchange Coupling of Nuclear Magnetic Moments by Conduction Electrons. *Physical Review*, 96(1):99–102, October 1954. 10.1103/PhysRev.96.99. URL https://link.aps.org/doi/10.1103/PhysRev.96.99. B

Kei Yosida. Magnetic Properties of Cu-Mn Alloys. *Physical Review*, 106(5):893–898, June 1957. 10.1103/PhysRev.106.893. URL https://link.aps.org/doi/10.1103/PhysRev.106.893. B

Appendix A

Appendix

A.1 From the logarithmic discretization to the Wilson's chain.

Logarithmic Discretization:

We start with an Anderson model Hamiltonian such as the one in (**??**) without magnetic field

$$H = \frac{U}{2} + \sum_{\sigma} \left[\left(\varepsilon_d + \frac{U}{2} \right) d_\sigma^\dagger d_\sigma + \frac{U}{2} (d_\sigma^\dagger d_\sigma - 1)^2 + \sum_{\mathbf{k}} \varepsilon_{\mathbf{k}} c_{\mathbf{k}\sigma}^\dagger c_{\mathbf{k}\sigma} + V_{\mathbf{k}} d_\sigma^\dagger c_{\mathbf{k}\sigma} + V_{\mathbf{k}}^* c_{\mathbf{k}\sigma}^\dagger d_\sigma \right]. \tag{A.1}$$

At low-energies we can assume that QD couples only to s-wave states in the leads[27]. This implies that that the Fermi surface is contained in a single, isotropic conduction band extending inside some fixed cutoffs $-D$ and D. Thus, $\varepsilon_{\mathbf{k}}$ only depends on $|\mathbf{k}|$. This makes possible to transform the sum over $\mathbf{k}$ in equation Equation A.1 into an integral over ε between the energy cutoffs

$$\begin{aligned} H \quad = \sum_\sigma \quad & \left[\left(\varepsilon_d + \frac{U}{2} \right) d_\sigma^\dagger d_\sigma + \frac{U}{2} (d_\sigma^\dagger d_\sigma - 1)^2 + \int_{-D}^{D} \mathrm{d}\varepsilon \; \varepsilon c_{\varepsilon\sigma}^\dagger c_{\varepsilon\sigma} \right. \\ & \left. + \int_{-D}^{D} \sqrt{\rho_\sigma(\varepsilon)} \mathrm{d}\varepsilon \; V_\varepsilon d_\sigma^\dagger c_{\mathbf{k}\sigma} + V_\varepsilon^* c_{\varepsilon\sigma}^\dagger d_\sigma \right]. \end{aligned} \tag{A.2}$$

Here $c_{\varepsilon\sigma}^\dagger$ creates an electron with energy ε and $\rho_\sigma(\varepsilon)$ is the density of states of the system per spin, which appears in the integral due to the change of variable from $\mathbf{k}$ to $\varepsilon \propto |\mathbf{k}|^2$. Finally, we ignore the energy dependence of ρ and V_d and we replace them by their values in the Fermi energy (This approximation has no great relevance which is justified in [27]) and we renormalize the energy band doing the replacements $k = \frac{\varepsilon}{D}$ and $c_{k\sigma} := \sqrt{D} c_{\varepsilon\sigma}$ so that (Equation A.2) becomes

$$H = D\sum_{\sigma}\left[\frac{1}{D}\left(\varepsilon_d+\frac{U}{2}\right)d^{\dagger}_{\sigma}d_{\sigma}+\frac{U}{2D}(d^{\dagger}_{\sigma}d_{\sigma}-1)^2+\int_{-1}^{1}\mathrm{d}k\; kc^{\dagger}_{k\sigma}c_{k\sigma}\right.$$
$$\left.+\sqrt{\frac{\Gamma}{\pi D}}\int_{-1}^{1}\mathrm{d}k\; d^{\dagger}_{\sigma}c_{k\sigma}+c^{\dagger}_{k\sigma}d_{\sigma}\right] \tag{A.3}$$
$$= H_d+D\sum_{\sigma}\left[\int_{-1}^{1}\mathrm{d}k\; kc^{\dagger}_{k\sigma}c_{k\sigma}+\sqrt{\frac{\Gamma}{\pi D}}\int_{-1}^{1}\mathrm{d}k\; d^{\dagger}_{\sigma}c_{k\sigma}+c^{\dagger}_{k\sigma}d_{\sigma}\right], \tag{A.4}$$

where $\Gamma=\pi\rho V^2$ is associated to the lever-width [28, (3.5)]. At this point we have our model dependent of three unit-less constants $\frac{\varepsilon_d}{D}$, $\frac{U}{2D}$ and $\frac{\Gamma}{\pi D}$. The logarithmic discretization starts by defining an scaling parameter $\Lambda\geq 1$ in diving the energy domain $[-1,1]$ into an array of intervals of the form $\{[\pm\Lambda^{-(n+1)},\pm\Lambda^{n}]\}_{n\in\mathbb{N}}$, as we can observe in **??**. Note that the width of these intervals is decreasing exponentially by

$$d_n=\Lambda^{-n}\left(1-\Lambda^{-1}\right).$$

Then inside of these energy intervals we can define a set of orthonormal Fourier series of the form

$$\phi^{\pm}_{np}(\varepsilon)=\begin{cases}\frac{1}{\sqrt{d_n}}e^{\pm i\omega_n p\varepsilon} & \varepsilon\in[\pm\Lambda^{-(n+1)},\pm\Lambda^{n}]\\ 0 & \text{a.o.c}\ ,\end{cases} \tag{A.5}$$

with $\omega_n:=\frac{2\pi}{d_n}$ so that $\phi^{\pm}_{np}\left(\pm\Lambda^{-(n+1)}\right)=\phi^{\pm}_{np}\left(\pm\Lambda^{-n)}\right)$. Then we can decompose the creation operators $c^{\dagger}_{k}$ into their interval-Fourier contributions as

$$c^{\dagger}_{k\sigma}=\sum_{np}\phi^{+}_{np}(k)c^{+\dagger}_{np\sigma}+\phi^{-}_{np}(k)c^{-\dagger}_{np\sigma} \tag{A.6}$$

with the new creation operators defined as

$$c^{\pm\dagger}_{np\sigma}:=\left(c^{\pm}_{np\sigma}\right)^{\dagger}=\int_{-1}^{1}\mathrm{d}\varepsilon\;\left[\phi^{+}_{np}(\varepsilon)\right]^{*}c^{\dagger}_{\varepsilon\sigma}.$$

This decomposition (Equation A.6) is a simple consequence of the orthonormality of the functions defined in (Equation A.5). In addition we can readily proof that $c^{\pm\dagger}_{np\sigma}$-operators satisfy the anti-commutation relations, so that they are rightful fermionic creation operators.

We can now use (Equation A.6) to replace the k-dependent terms in hamiltonian (Equation A.3). Then we obtain

$$\begin{aligned}
\int_{-1}^{1} \mathrm{d}k\, c^{\dagger}_{k\sigma} d_{\sigma} &= \int_{-1}^{1} \mathrm{d}k \left(\sum_{np} \phi^{+}_{np}(k) c^{+\dagger}_{np\sigma} + \phi^{-}_{np}(k) c^{-\dagger}_{np\sigma} \right) d_{\sigma} \\
&= \left(\sum_{np} \left(\int_{-1}^{1} \mathrm{d}k\, \phi^{+}_{np}(k) \right) c^{+\dagger}_{np\sigma} + \left(\int_{-1}^{1} \mathrm{d}k\, \phi^{-}_{np}(k) \right) c^{-\dagger}_{np\sigma} \right) d_{\sigma} \\
&= \left(\sum_{np} \left(\int_{\Lambda^{-(n+1)}}^{\Lambda^{-n}} \mathrm{d}k\, \frac{e^{i\omega_n pk}}{\sqrt{d_n}} \right) c^{+\dagger}_{np\sigma} + \left(\int_{-\Lambda^{-n}}^{-\Lambda^{-(n+1)}} \mathrm{d}k\, \frac{e^{-i\omega_n pk}}{\sqrt{d_n}} \right) c^{-\dagger}_{np\sigma} \right) d_{\sigma} \\
&= \left(\sum_{np} \sqrt{d_n} \delta_p c^{+\dagger}_{np\sigma} + \sqrt{d_n} \delta_p c^{-\dagger}_{np\sigma} \right) d_{\sigma} \\
&= \sqrt{1-\Lambda^{-1}} \sum_{n} \Lambda^{-\frac{n}{2}} \left(c^{+\dagger}_{np\sigma} + c^{-\dagger}_{np\sigma} \right) d_{\sigma}. \qquad \text{(A.7)}
\end{aligned}$$

And

$$\begin{aligned}
\int_{-1}^{1} \mathrm{d}k\, k c^{\dagger}_{k\sigma} c_{k\sigma} &= \sum_{n,n',p,p'} \sum_{s,s'=\pm} \left(\int_{-1}^{1} k \mathrm{d}k\, \phi^{s}_{np}(k) \left(\phi^{s'}_{np}(k) \right)^{*} \right) c^{s\dagger}_{np\sigma} c^{s'}_{n'p'\sigma} \\
&= \sum_{n,n',p,p'} \sum_{s,s'=\pm} \left(\frac{\delta_{nn'}\delta_{ss'}}{d_n} \int_{\Lambda^{-(n+1)}}^{\Lambda^{-n}} k \mathrm{d}k\, e^{is\omega_n k(p-p')} \right) c^{s\dagger}_{np\sigma} c^{s}_{np'\sigma} \\
&= \sum_{npp'} \sum_{s=\pm} \left(\frac{s}{2} \Lambda^{-2n} \left(1-\Lambda^{-2} \right) \delta_{pp'} + \frac{1-\delta_{pp'}}{is\omega_n (p-p')} \left[k e^{is\omega_n k(p-p')} \right]_{\Lambda^{-(n+1)}}^{\Lambda^{-n}} \right) \frac{c^{s\dagger}_{np\sigma} c^{s'}_{np'\sigma}}{d_n} \\
&= \frac{1}{2} \left(1+\Lambda^{-1} \right) \sum_{np} \Lambda^{-n} \left(c^{+\dagger}_{np\sigma} c^{+}_{np\sigma} - c^{-\dagger}_{np\sigma} c^{-}_{np\sigma} \right) \\
&\qquad + \sum_{n} \sum_{p \neq p'} \frac{1-\Lambda^{-1}}{2i\pi (p'-p)} \left(c^{+\dagger}_{np\sigma} c^{+}_{np'\sigma} - c^{-\dagger}_{np'\sigma} c^{-}_{np\sigma} \right) e^{\frac{2i\pi(p-p')}{1-\Lambda^{-1}}}. \qquad \text{(A.8)}
\end{aligned}$$

Thus, if we replace (Equation A.7) and (Equation A.8) into (Equation A.3) we will obtain a logarithmic discretization of the hamiltonian. The next part will we to map this discretization to an iterative process that is worth for a numerical computations.

Mapping the Anderson model to a Chain-Hamiltonian

We are looking for a model just like the one we have in the right part of **??**. This is because a Chain-Hamiltonian will give an iterative approximation of the Anderson model with an increasing (but still controllable) number of degrees of freedom. This will provide the rightful structure for a numerical diagonalization of the hamiltonian.

To do this, observe from equations (Equation A.7),(Equation A.8) that the QD (d_σ) couples directly only to the operators with $p=0\left(c^{\pm\dagger}_{n0\sigma}\right)$. The $p\neq 0$ terms will appear in the hamiltonian only because they are coupled to $c^{+\dagger}_{np\sigma}$ in Equation (Equation A.8). Thus, as a first approximation we can neglect all terms in (Equation A.8) with $p\neq 0$. This leaves only the first part of (Equation A.8), so that we can define $c^{\pm\dagger}_{n\sigma}:=c^{\pm\dagger}_{np\sigma}$. Let

$$f^\dagger_{0\sigma}=\sqrt{\frac{1-\Lambda^{-1}}{2}}\sum_n \Lambda^{-\frac{n}{2}}\left(c^{+\dagger}_{n\sigma}+c^{-\dagger}_{n\sigma}\right),\ \text{so that}\ \sqrt{2}f^\dagger_{0\sigma}d_\sigma=\int_{-1}^{1}\mathrm{d}k\ c^\dagger_{k\sigma}d_\sigma. \tag{A.9}$$

Note $\left\{f^\dagger_{0\sigma},f_{0\sigma}\right\}=\frac{1-\Lambda^{-1}}{2}\sum_n 2\Lambda^{-n}=1$. Replacing this in (Equation A.3)we get

$$H=H_d+D\sum_\sigma\left[\sqrt{\frac{2\Gamma}{\pi D}}\left(d^\dagger_\sigma f_{0\sigma}+f^\dagger_{0\sigma}d_\sigma\right)+\frac{1}{2}\left(1+\Lambda^{-1}\right)\sum_n\Lambda^{-n}\left(c^{+\dagger}_{n\sigma}c^{+}_{n\sigma}-c^{-\dagger}_{n\sigma}c^{-}_{n\sigma}\right)\right].$$

$f^\dagger_0$will represent the first site of the chain-hamiltonian in **??** since no other term is coupled to the dot hamiltonian. We also have the coupling term $\xi_0=\sqrt{\frac{2\Gamma}{\pi D}}$. It is possible to obtain the following $f^\dagger_m$-operators by supposing a solution of the form

$$f^\dagger_{m\sigma}=\sum_n a^+_{mn}c^{+\dagger}_{n\sigma}+a^-_{mn}c^{-\dagger}_{n\sigma}=\sum_n\sum_{s=\pm}a^s_{mn}c^{s\dagger}_{n\sigma}, \tag{A.10}$$

such that they satisfy the anti-commutation relations

$$\left\{f^\dagger_{m\sigma},f_{m\sigma}\right\}=\delta_{mm'}\delta_{\sigma\sigma'}\ ,\ \left\{f^\dagger_{m\sigma},f^\dagger_{m\sigma}\right\}=\left\{f^\dagger_{m\sigma},f^\dagger_{m\sigma}\right\}=0$$

and

$$\frac{1}{2}\left(1+\Lambda^{-1}\right)\sum_n\Lambda^{-n}\left(c^{+\dagger}_{n\sigma}c^{+}_{n\sigma}-c^{-\dagger}_{n\sigma}c^{-}_{n\sigma}\right)=\sum_{m=0}^{\infty}\Lambda^{\frac{-m}{2}}\xi_m\left(f^\dagger_{m\sigma}f_{m+1,\sigma}+f^\dagger_{m+1\sigma}f_{m\sigma}\right). \tag{A.11}$$

It is possible to find a solution for this system using the formula of the right part of equation Equation A.11. Since the relation is only given between consecutive terms $m,m+1$ and we already have the coefficients for $m=0$ $\left(a^s_{0n}=\sqrt{\frac{1-\Lambda^{-1}}{2}}\Lambda^{-\frac{n}{2}}\right)$. Then it is possible to determine the upper coefficients in a recursive way starting from $m=0$. Supposing we can obtain the m^{th}-coefficients (a^s_{mn}) and then finding iteratively the coefficients of $m+1$ (a^s_{mn}) using the relation given by equation (Equation A.11). This provides a numerical way for obtaining the $f^\dagger_{m\sigma}$ operators. In fact in our case, where we actually did important assumptions, the problem can be solved analytically obtaining that the final Hamiltonian is given by

$$H=H_d+D\sum_\sigma\left[\sqrt{\frac{2\Gamma}{\pi D}}\left(d^\dagger_\sigma f_{0\sigma}+f^\dagger_{0\sigma}d_\sigma\right)+\frac{1}{2}\left(1+\Lambda^{-1}\right)\sum_{n=0}^{\infty}\Lambda^{\frac{-n}{2}}\xi_n\left(f^\dagger_{n\sigma}f_{n+1,\sigma}+f^\dagger_{n+1\sigma}f_{n\sigma}\right)\right]. \tag{A.12}$$

with

$$\xi_n = \frac{1-\Lambda^{-n-1}}{\left(1-\Lambda^{-2n-1}\right)^{\frac{1}{2}}\left(1-\Lambda^{-2n-3}\right)^{\frac{1}{2}}}.$$

The formal recursive-solution of this problem can be found in [29] . Note that equation (Equation A.12) describes the chain hamiltonian model that we where looking for in **??**. Note that in the limit when $n \longrightarrow \infty$

$$\Lambda^{\frac{-n}{2}}\xi_n \longrightarrow \frac{\Lambda^{\frac{-n}{2}}\left(1-\Lambda^{-n}\right)}{1-\Lambda^{-2n}} \sim \frac{\Lambda^{\frac{-n}{2}}}{1+\Lambda^{-n}},$$

which implies an exponential decaying of the hopping term in the chain.

Appendix B

Three peak appearance in the Double Quantum Dot model.

The DQD model is characterized by the formation of a new state that entangles the two Quantum dots through the leads. This produces an anti-ferromagnetic interaction between the QDs, commonly known as Ruderman-Kittel-Kasuya-Yosida (RKKY) interaction [30, 31]. As consequense, two satelite peaks will emerge in the Density of States.

To explain this phenomenon we will take a symmetric version of Hamiltonian (**??**) with $2e_i = U_i = U$, $t_i = t$ and $t_{dots} = 0$ for $i \in \{1,2\}$.

$$H = \sum_{i,k,\sigma} \frac{U_i}{2}(d^\dagger_{i\sigma}d_{i\sigma} - 1)^2 + t(d_{+,\downarrow} + d^\dagger_{+,\downarrow})\gamma_1 + \Gamma_i(d^\dagger_{i\sigma}c_{k\sigma} + c^\dagger_{k\sigma}d_{i\sigma}). \tag{B.1}$$

The symmetry of the previous Hamiltonian is suitable to apply a base change of the form

$$d_{+,\sigma} = \frac{1}{\sqrt{2}}(d_{1\sigma} + d_{2\sigma}) \ , \ d_{-,\sigma} = \frac{1}{\sqrt{2}}(d_{1\sigma} - d_{2\sigma}).$$

These new operators satisfy the fermionic anti-commutation relations

$$\{d_{\pm,\sigma}, d^\dagger_{\pm,\sigma}\} = 1, \{d_{\pm,\sigma}, d^\dagger_{\mp,\sigma}\} = 0,$$

so that the may be considered as fermion operators. All lineal terms in (Equation B.1) are trivially adapted to the new base. The repulsion potential

$$\sum_i (\sum_\sigma d^\dagger_{i\sigma}d_{i\sigma} - 1)^2 = (\sum_\sigma d^\dagger_{1\sigma}d_{1\sigma} - 1)^2 + (\sum_\sigma d^\dagger_{2\sigma}d_{2\sigma} - 1)^2.$$

gives rise to a non-trivial interaction between the new states. To find this interaction we define the particle number operator

$$\hat{n}_{i,\sigma} := d^\dagger_{i,\sigma}d_{i,\sigma}.$$

So that

$$\hat{n}_{1,\sigma} = \frac{1}{2}\left(\hat{n}_{+,\sigma} + \hat{n}_{-,\sigma} + d^\dagger_{+,\sigma}d_{-,\sigma} + d^\dagger_{-,\sigma}d_{+,\sigma}\right) = \frac{1}{2}\left(\hat{N}_\sigma + \hat{E}_\sigma\right),$$

with $\hat{N} = \hat{n}_{+,\sigma} + \hat{n}_{-,\sigma}$ and $\hat{E}_\sigma = d^\dagger_{+,\sigma}d_{-,\sigma} + d^\dagger_{-,\sigma}d_{+,\sigma}$. Similarly

$$\hat{n}_{2,\sigma} = \frac{1}{2}\left(\hat{N}_\sigma - \hat{E}_\sigma\right).$$

Hence

$$\sum_i (\sum_\sigma d^\dagger_{i\sigma} d_{i\sigma} - 1)^2 = \left(\frac{\hat{N}+\hat{E}}{2} - 1\right)^2 + \left(\frac{\hat{N}-\hat{E}}{2} - 1\right)^2 = \frac{\left(\hat{N}-2\right)^2 - \hat{E}^2}{2},$$

with $\hat{N} = \sum_\sigma \hat{N}_\sigma$, $\hat{E} = \sum_\sigma \hat{E}_\sigma$. Note that opeator $\hat{N}$ represents the total occupation number inside both dots. If this occupation is different than 2 there is an imbalance between particles and dots that is punished by this term. The term E^2 is much more interesting since this one is the responsible for the emergence of satellite peaks in the DOS. To understand what it makes it is simple to observe its results when applied to a based ordered by $|+,-\rangle$.

$$\hat{E}^2|\uparrow,0\rangle = \hat{E}|0,\uparrow\rangle = |\uparrow,0\rangle$$

$$\hat{E}^2|\uparrow,\downarrow\rangle = \hat{E}\left(|0,\uparrow\downarrow\rangle + |\uparrow\downarrow,0\rangle\right) = 2|\uparrow,\downarrow\rangle - 2|\downarrow,\uparrow\rangle$$

The new Hamiltonian

$$H = \sum_\sigma \frac{U}{4}\left(\left(\hat{N}-2\right)^2 - \hat{E}^2\right) + \frac{t}{\sqrt{2}}(d_{+,\downarrow} + d^\dagger_{+,\downarrow})\gamma_1 + \frac{\Gamma}{\sqrt{2}}\sum_k (d^\dagger_{+,\sigma} c_{k\sigma} + c^\dagger_{k\sigma} d_{+,\sigma}) \tag{B.2}$$

is represented in **??**

We can explain this three-peak as the result of a new strong coupling interaction characterized by the spin exchange between both dots.

In addition, the spin-up DOS at the Fermi energy grows faster than the spin-down DOS, breaking the initial spin-symmetry when $t_1 = t_2 = 0$. At $t_1 = t_2 = 0.02D$ the spin-up DOS at the fermi energy doubles the spin-down DOS which implies that the Majorana signature is present in both dots. Indeed **??** shows that the relation $\frac{\rho_\uparrow(0)}{\rho_\uparrow(0)}$ increases continuously from 1 to 2. Note that the Majorana is completely attached when the coupling t_1 reaches the order of $0.01D$.

B.1 Initial DQD-Majorana Hamiltonian.

$H_{N_\uparrow=0,P_\downarrow=-1}$:

$$\begin{array}{l} |\downarrow,\downarrow,\downarrow\rangle \rightarrow \\ |0,0,\downarrow\rangle \rightarrow \\ |0,\downarrow,0\rangle \rightarrow \\ |\downarrow,0,0\rangle \rightarrow \end{array} \begin{bmatrix} \varepsilon_d^+ + \frac{U^+}{2} - 2h + \varepsilon_m & 0 & -\tilde{t}_{+1} & \tilde{t}_{+2} \\ 0 & \frac{U^+}{2} + \varepsilon_m & \tilde{t}^*_{-2} & \tilde{t}^*_{-1} \\ -\tilde{t}^*_{+1} & \tilde{t}_{-2} & \varepsilon_{d_2} + \frac{U^+}{2} - h - \varepsilon_m & t \\ \tilde{t}^*_{+2} & \tilde{t}_{-1} & t^* & \varepsilon_{d_1} + \frac{U^+}{2} - h - \varepsilon_m \end{bmatrix}$$

$H_{N_\uparrow=0,P_\downarrow=1}$:

$$\begin{array}{c} |0,0,0\rangle \to \\ |\downarrow,\downarrow,0\rangle \to \\ |\downarrow,0,\downarrow\rangle \to \\ |0,\downarrow,\downarrow\rangle \to \end{array} \begin{bmatrix} \frac{U^+}{2}-\varepsilon_m & 0 & \tilde{t}_{+1} & \tilde{t}_{+2} \\ 0 & \varepsilon_d^+ + \frac{U^+}{2} - 2h - \varepsilon_m & \tilde{t}^*_{-2} & -\tilde{t}^*_{-1} \\ \tilde{t}^*_{+1} & \tilde{t}_{-2} & \varepsilon_{d_1} + \frac{U^+}{2} - h + \varepsilon_m & t \\ \tilde{t}^*_{+2} & -\tilde{t}_{-1} & t^* & \varepsilon_{d_2} + \frac{U^+}{2} - h + \varepsilon_m \end{bmatrix}$$

$H_{N_\uparrow=2,P_\downarrow=-1}$:

$$\begin{array}{c} |\uparrow\downarrow,\uparrow\downarrow,\downarrow\rangle \to \\ |\uparrow,\uparrow,\downarrow\rangle \to \\ |\uparrow,\uparrow\downarrow,0\rangle \to \\ |\uparrow\downarrow,\uparrow,0\rangle \to \end{array} \begin{bmatrix} 2\varepsilon_d^+ + \frac{3U^+}{2} + \varepsilon_m & 0 & \tilde{t}_{+1} & \tilde{t}_{+2} \\ 0 & \varepsilon_d^+ + \frac{U^+}{2} + 2h + \varepsilon_m & \tilde{t}^*_{-2} & -\tilde{t}^*_{-1} \\ \tilde{t}^*_{+1} & \tilde{t}_{-2} & f(d_1,d_2) + h - \varepsilon_m & -t \\ \tilde{t}^*_{+2} & -\tilde{t}_{-1} & -t^* & f(d_2,d_1) + h - \varepsilon_m \end{bmatrix}$$

with $f(d_i,d_j) = \varepsilon_{d_i} + \frac{U_i}{2} + 2\varepsilon_{d_j} + \frac{3U_j}{2}$.

$H_{N_\uparrow=2,P_\downarrow=1}$:

$$\begin{array}{c} |\uparrow,\uparrow,0\rangle \to \\ |\uparrow\downarrow,\uparrow\downarrow,0\rangle \to \\ |\uparrow\downarrow,\uparrow,\downarrow\rangle \to \\ |\uparrow,\uparrow\downarrow,\downarrow\rangle \to \end{array} \begin{bmatrix} \varepsilon_d^+ + \frac{U^+}{2} + 2h - \varepsilon_m & 0 & -\tilde{t}_{+1} & \tilde{t}_{+2} \\ 0 & 2\varepsilon_d^+ + \frac{3U^+}{2} - \varepsilon_m & \tilde{t}^*_{-2} & \tilde{t}^*_{-1} \\ -\tilde{t}^*_{+1} & \tilde{t}_{-2} & f(d_2,d_1) + h + \varepsilon_m & -t \\ \tilde{t}^*_{+2} & \tilde{t}_{-1} & -t^* & f(d_1,d_2) + h + \varepsilon_m \end{bmatrix}$$